Rev. Adv. Mater. Sci. 41 (2015) 72-83

INTERPRETING THE INTERNAL LENGTH SCALE IN STRAIN GRADIENT PLASTICITY

Xu Zhang[1] and Katerina Aifantis[2,3]

[1]Applied Mechanics and Structure Safety Key Laboratory of Sichuan Province, School of Mechanics and Engineering, Southwest Jiaotong University, Chengdu 610031, China
[2]Civil Engineering–Engineering Mechanics, University of Arizona, Tucson, AZ, USA
[3]Modern Functional Materials Chair, ITMO University, Lomonosova 9, St. Petersburg, 191002, Russia

Received: March 13, 2015

Abstract. Gradient plasticity frameworks arise from the consideration of the gradient of the plastic strain as an independent variable. In doing so a new material parameter, the internal length (or gradient coefficient) is introduced, which governs the gradient effects. Despite the efficiency of these theories, there does not exist a unified interpretation of the internal length, and its relationship with the material microstructure has not been clearly understood. The present article provides a review on the various interpretations that recent studies have provided for the internal length that go beyond fitting it to experimental data.

1. INTRODUCTION

Strain gradient plasticity has become one of the most popular continuum mechanics frameworks as it allows for numerous mechanics phenomena to be interpreted, such as the dependence of the strength on the grain and specimen size (size effects) [1-3], the inverse Hall-Petch behavior [4-6], the behavior of micropillars [7-10] and the shear band spacing [11-16]. Attempts to capture such behaviors with classical continuum plasticity theory were not successful as it does not possess an intrinsic material length-scale that allows the microstructure to be accounted for. It was this lack of classical theories to account for the behavior of the neighboring material volumes that motivated Aifantis in 1984 [11] to consider the gradient of the plastic strain as an independent variable. In doing so, a gradient coefficient was necessary for dimensional consistency and as it had units of length it is often referred to as the internal length scale. Initially, gradient theories were used to predict the shear band spacing [13-16] and dispense with the mesh dependence in finite element calculations [17]. With the torsion experiments of Fleck et al. in 1994 [18] which indicated size effects in the stress-strain curve as the diameter decreased, strain gradient plasticity models began to be extensively employed for explaining the size dependent mechanical behavior of materials at the micron- and submicron- scales.

The effect of the plastic strain gradient becomes significant when the length associated with the deformation field is reduced to be of similar order as the characteristic internal length scale. Therefore, the value of the internal length scale plays a significant role within all strain gradient plasticity frameworks.

In spite of the success of strain gradient plasticity theories, one main drawback is that the internal length scale is introduced as a phenomenological coefficient which is determined by fits to experimental data [19]. It has been proposed that the internal length scales depend on the loading situation rather than being intrinsic [20], leading to the conclusion that it should be related with the underlying deformation mechanisms and microstructure [1]. However, the physical origin of the internal length scale in strain gradient theories is not clear, and its con-

Corresponding author: Katerina Aifantis, e-mail: aifantis@email.arizona.edu

nection to the material microstructure is still at best tenuous.

In the last decade, many researchers have aimed to establish a relationship between the internal length scale and the dislocation structure or the microstructure. Specifically, the internal length scale has been related with the dislocation source length, dislocation mean spacing, pile-ups in front of grain boundaries, grain size, slip zones and specimen size. This review summarizes these works in hopes of motivating further research in this significant and unresolved topic.

The paper is organized as follows: First, we briefly describe how internal length scales are introduced into the existing popular strain gradient frameworks. Then the recent progress on exploring the physical explanation and microstructural correlation of internal length scales is given.

2. INTERNAL LENGTH SCALES IN STRAIN GRADIENT PLASTICITY FRAMEWORK

The works of Aifantis [1,12] were the first to include strain gradients into the plasticity framework. He proposed the theory based upon the ideas of thermal activated diffusion of dislocations under potential gradients. The Aifantis theory gives a flow stress expressed as a function of the plastic shear strain $\gamma^p = \sqrt{2\varepsilon'_{ij}\varepsilon'_{ij}}$ (ε'_{ij} denotes the deviatoric plastic strain) as

$$\tau = \kappa(\gamma^p) - c\nabla^2\gamma^p, \tag{1}$$

where κ is the hardening function and c is the gradient coefficient, which is required for dimensional consistency. The first term in the right side of Eq. (1) denotes the classic rate-independent flow rule, and the second term accounts for the nonlocal contribution. These two contributions to hardening are coupled through the gradient coefficient c. The gradient-dependent flow stress given by Eq. (1) can be generalized further by considering the effect of the first-order strain gradients and allowing the gradient coefficients to be strain dependent. In the generalized Aifantis gradient plasticity theory [31], the effective Von Mises stress $\bar{\sigma} = \sqrt{2/3\sigma'_{ij}\sigma'_{ij}}$ (σ'_{ij}: deviatoric Cauchy stress) is related with the effective strain $\bar{\varepsilon} = \sqrt{2/3\varepsilon'_{ij}\varepsilon'_{ij}}$ as

$$\bar{\sigma} = \kappa(\bar{\varepsilon}) + c_1(\bar{\varepsilon})(\nabla\bar{\varepsilon}\cdot\nabla\bar{\varepsilon})^m + c_2(\bar{\varepsilon})\nabla^2\bar{\varepsilon}, \tag{2}$$

where $c_1(\bar{\varepsilon})$ and $c_2(\bar{\varepsilon})$ are strain dependent gradient coefficients. If $c_1(\bar{\varepsilon}) = 0$, Eq. (2) will degenerate into the earlier simpler version of Aifantis's model as given in Eq. (1). The usual homogeneous hardening can be described through the power-law hardening, i.e.

$$\kappa(\bar{\varepsilon}) = \kappa_0\bar{\varepsilon}^n, \tag{3}$$

where κ_0 and n is the hardening exponent.

About a decade later, Fleck et al. [18] developed a phenomenological strain gradient plasticity theory within the couple stress framework [21]. They defined a generalized effective strain using a single and constant internal length scale as

$$E = \varepsilon_e^2 + l^2\chi_e^2 = \frac{2}{3}\varepsilon_{ij}\varepsilon_{ij} + l^2\frac{2}{3}\chi_{ij}\chi_{ij}, \tag{4}$$

where $\varepsilon_e = \sqrt{2\varepsilon_{ij}\varepsilon_{ij}/3}$ is an effective measure of the strain tensor ε_{ij}, and $\chi_e = \sqrt{2\chi_{ij}\chi_{ij}/3}$ is an effective measure of the curvature tensor χ_{ij}. Here they called the gradient coefficient internal length and denoted it as l. It should be noted that they did not consider a formal distinction between the elastic and plastic components of the displacement and strain [18]. Thus, there is a fictitious representation of the elastic behavior where the internal length scale is artificially present [2]. In order to remedy this, a reformulation of the Fleck-Hutchinson framework [2] was established in the manner in which elastic and plastic strains are decomposed. In doing so they argued that at least two internal length scales were needed in order to account for heterogeneous deformation; one l characterizing stretch gradients and the other accounting for rotation gradients (or sharing gradients). However, after numerous re-formulations, Fleck-Hutchinson [2] proposed a framework which was essentially the counterpart of the Aifantis model for deformation plasticity, and again only one internal length scale was employed. Particularly, in the deformation theory framework of the Fleck-Hutchinson model in 2001, they defined a potential energy as [2],

$$\Psi(u_i,\varepsilon_{\mathrm{p}}) = \int_V \left\{ \frac{1}{2}C_{ijkl}\left(\varepsilon_{ij} - \varepsilon_{\mathrm{p}}m_{ij}\right)\left(\varepsilon_{kl} - \varepsilon_{\mathrm{p}}m_{kl}\right) + \int_0^{E_p}\sigma(\tilde{\varepsilon}_{\mathrm{p}})\,\mathrm{d}\tilde{\varepsilon}_{\mathrm{p}} \right\}\mathrm{d}V - \int_{S_T}\left(T_i^0u_i + t^0\varepsilon_{\mathrm{p}}\right)\mathrm{d}S, \tag{5}$$

where C_{ijkl} is the elastic stiffness tensor, $\sigma(\tilde{\varepsilon}_{\mathrm{p}})$ denotes the uniaxial tensile stress–strain curve of the material; S_T is the portion of the surface where the traction T_i^0 and higher-order traction t^0 (resulting from strain gradients) are prescribed. Here, the plastic strain tensor $\varepsilon_{ij}^{\mathrm{p}}$ is related with the effective plastic

strain ε_p as $\varepsilon_{ij}^p = \varepsilon_p m_{ij}$. The direction m_{ij} of the plastic strain is co-directional with the stress deviator: $m_{ij} = 3\sigma'_{ij}/2\bar{\sigma}$. The first term in the volume integral of Eq. (5) represents the elastic work density while the second accounts for the plastic work density, and the third term is the work done on the external surface. It should be noted that the plastic potential is evaluated at the generalized effective plastic strain E_P rather than ε_p. In 1-D E_P was defined as [2]

$$(E^p) = (\varepsilon^p)^2 + l^2 \varepsilon^p_{,i} \varepsilon^p_{,i}, \tag{6}$$

while the elaborate version employing three internal length scales can be found in [2]. The first part of Eq. (6) represents the classical hardening resulting from statistically stored dislocations (SSDs), while the second term represents the hardening from geometrically necessary dislocations (GNDs). It's to be emphasized that the SSD density ρ_S characterizes the deformation field which is macroscopilly uniform, thus is related with the plastic strain ε_p, while the GND density ρ_G characterizes the heterogeneous deformation field accompanying the plastic strain gradient $\varepsilon^p_{,i}$. The similar form of the homogeneous hardening and heterogeneous hardening indicated that the hardening effect from GNDs and SSDs was assumed to occur in the same manner. When the strain gradient effect is significant, the GND density can overcome the SSD density, and the hardening contribution is dominated by GNDs [18]. In the classical plasticity model, it is tacitly assumed that the GND density ρ_G is smaller than SSD density ρ_S, thus no length scale enters into the framework [18]. Eq. (6) will degenerate into the classical linear hardening case when either the internal length scale is set to be zero, or the strain gradient is weaker when the length of the heterogeneous deformation field is larger compared to the internal length scale (such as in the case of macroscale deformation).

Later, in order to eliminate the implicit involvement of the direction of the stress deviator σ'_{ij}, Fleck and Willis modified Eq. (5) as

$$\Psi(u_i, \varepsilon^p_{ij}) = \int_V \left\{ U\left(\varepsilon_{ij}, \varepsilon^p_{ij}, \varepsilon^p_{ij,k}\right) \right\} \mathrm{d}V - \int_{S_T} \left(T_i^0 u_i + t_{ij}^0 \varepsilon^p_{ij} \right) \mathrm{d}S, \tag{7}$$

where

$$U(\varepsilon_{ij}, \varepsilon^p_{ij}, \varepsilon^p_{ij,k}) = \frac{1}{2} C_{ijkl} \left(\varepsilon_{ij} - \varepsilon^p_{ij}\right)\left(\varepsilon_{kl} - \varepsilon^p_{ij}\right) + V(\varepsilon^p_{ij}, \varepsilon^p_{ij,k}). \tag{8}$$

The plastic potential V was taken as

$$V(\varepsilon^p_{ij}, \varepsilon^p_{ij,k}) = \int_0^{E_p} \sigma(\bar{\varepsilon}_p)\, \mathrm{d}\bar{\varepsilon}_p, \tag{9}$$

and with Eq. (6) being replaced by

$$E^p = \sqrt{\frac{2}{3}\left[\varepsilon^p_{ij}\varepsilon^p_{ij} + l^2 \varepsilon^p_{ij,k}\varepsilon^p_{ij,k}\right]}. \tag{10}$$

In addition to the Aifantis and Fleck-Hutchinson-Willis frameworks numerous researchers have formulated their own gradient plasticity framework [22-26]. Among these one distinguishes the work of Gurtin and Anand [27] who proved that the initial Fleck-Hutchinson frameworks [2] are not thermodynamically consistent while the Aifantis models [11,12,etc.] are. A step beyond the initial gradient plasticity frameworks was done by Gudmundson [25] and Aifantis-Willis [28,29] who introduced a new interfacial energy term into the gradient-dependent energy functional. In [25] this interface energy was a function of the shear modulus and a length scale related to the interface, while in [28,29] an explicitly new interface energy, that dependent upon the ability of interfaces to deform was introduced as

$$\Psi(u_i, \varepsilon^p_{ij}) = \int_V \left\{ U\left(\varepsilon_{ij}, \varepsilon^p_{ij}, \varepsilon^p_{ij,k}\right) \right\} \mathrm{d}V + \int_\Gamma \phi(\varepsilon^p_{ij})\, \mathrm{d}\Gamma - \int_{S_T} \left(T_i^0 u_i + t_{ij}^0 \varepsilon^p_{ij} \right) \mathrm{d}S, \tag{11}$$

where $\phi(\varepsilon^p_{ij})$ is the interface energy.

It is seen that all terms that come into play in gradient theories have been well studied aside from the internal length, and interface energy. From these terms, the internal length has been studied the most. Initially, the most common technique to obtain its value was by fitting gradient plasticity derived hardness expressions to nanoindentation hardness data [1,22,30]. However, these works do not provide physical insight into the origin of the internal length, but rather show its dependence on the indenter geometry. In [30] an initial interpretation for the internal length dependence was done since it was stated that hardest materials had the smallest values of l. Since the free slip distance of dislocations decreases with hardness, this suggested that l was related to the free slip distance. Since then numerous elaborate studies that try to understand the origin of the internal length have been performed and are summarized below.

3. CONNECTION WITH DISLOCATION SPACING

Although in most gradient theories the internal length (gradient coefficient) is treated as a constant it was

proposed as described in Eq. (2) [31] that the gradient coefficient can depend on the strain. In [31] they set c_1=0 in Eq. (2) and proposed that c_2 decreased with increasing strain. This was achieved by employing a phenomenological relation for c_2 that related the gradient coefficient to the plastic strain and hardening exponent (n) as

$$c_2(\bar{\varepsilon}) = c_0 \bar{\varepsilon}^{n-1}, \tag{12}$$

where c_o is the gradient coefficient at shear strain equal to 1. It is noted that the gradient coefficient was related to the internal length scale as $c_0=k_0 l_0^2$, where l_0 is the internal length at shear strain equal to 1 and κ_0 is the hardening modulus. Eq. (12) allowed for successful modeling of the torsion size effects in Cu wires [31], and hence motivated further work that employed a variable internal length during deformation. These works [24,39,40] are summarized below.

3.1. Relating the internal length to the dislocation spacing using flow theory

In [24] using a flow version of gradient plasticity it was found that the internal length can vary during deformation as a function of the dislocation spacing L_S by using Taylor's hardening law. Microscopically the Taylor equation gives the overall flow stress τ_f in term of the total dislocation density ρ_T [24] as

$$\sigma_f = Z\partial_S G b_S \sqrt{\rho_T}, \tag{13}$$

where Z is the Taylor factor, b_S and ∂_S are the magnitudes of the Burgers vector and statistical coefficient associated with SSDs respectively, and G is the shear modulus. An equivalent total dislocation density was given by

$$\rho_T = \left[\rho_S^{\beta/2} + \left(\frac{\partial_G b_G}{\partial_S b_S} \right)^{\beta} \rho_G^{\beta/2} \right]^{2/\beta}, \tag{14}$$

where b_G and ∂_G are the magnitudes of the Burgers vector and statistical coefficients associated with GNDs respectively, ρ_G and ρ_S are the densities of GNDs and SSDs, respectively, which are coupled through the interaction coefficient β. The GND density was related with the effective strain gradient η as

$$\rho_S = \frac{\eta \bar{r}}{b_G}. \tag{15}$$

and the SSDs density was related with the effective plastic strain ε_P and dislocation mean spacing L_S as

$$\rho_G = \frac{\varepsilon_p}{b_S L_S \bar{M}}. \tag{16}$$

In Eqs. (15) and (16), $\bar{M}$ and $\bar{r}$ are the Schmidt's orientation factor and Nye factor respectively [24]. Substitution of Eqs. (15) and (16) into Eq. (13) yielded

$$\sigma_f = \frac{Z\partial_S G b_S}{\sqrt{b_S L_S \bar{M}}} \left[\varepsilon_p^{\beta/2} + \left(\frac{\partial_G^2 b_G L_S \bar{M} \bar{r}}{\partial_S^2 b_S} \eta \right)^{\beta/2} \right]^{1/\beta}. \tag{17}$$

Alternatively, the phenomenological gradient plasticity expression for the flow stress was written in [24] as

$$\sigma_f = \sigma_0 \left[\varepsilon_p^r + (l\eta)^r \right]^{n/r}, \tag{18}$$

where σ_0 and η are the yield stress and hardening exponent in uniaxial tension, and r is an interaction coefficient (between the effective plastic strain ε_p and the effective strain gradient η). Comparing the Taylor based flow stress of Eqs. (17) with the phenomenological gradient plasticity expression for the flow stress of Eq. (18) gave the internal length and yield stress as

$$l = \frac{\partial_G^2 b_G L_S \bar{M} \bar{r}}{\partial_S^2 b_S} \tag{19}$$

and

$$\sigma_0 = \frac{Z\partial_S G b_S}{\sqrt{b_S L_S \bar{M}}}. \tag{20}$$

Since both l and σ_0 were related to the dislocation spacing, combination of Eq. (19) and (20) gave an alternative expression of the internal length scale as a function of σ_0 as

$$l = Z^2 \partial_G^2 b_G \bar{r} \left(\frac{G}{\sigma_0} \right)^2. \tag{21}$$

Thus, the internal length scale was predicted to be smaller for work-hardened specimen since the dislocation mean spacing is smaller due to the initially higher dislocation density. These results were consistent with fitting gradient plasticity expressions to indentation tests, since the fits gave a smaller internal length in work hardened oxygen free copper (OFC) than in annealed OFC [24]. The comparison of the internal length scales obtained from

Table 1. Dependence of Internal length-scale on strain level and hardening exponents, which are obtained from micro- and nano-indentation experiments on different materials with different indenters.

	Hardening exponents 1/*n*	Spherical indenter at plastic strain level of 0.01	Pyramidal indenter at plastic strain level of 0.07
Annealed iridium [57,58]	8.9	0.52	0.17
Annealed OFC [59,60]	2	0.79	0.37

spherical indentation which was determined at a specific plastic strain level of 0.01 were smaller than those from pyramidal indentation determined at a strain level of 0.07 as shown in Table 1 (obtained in [24]). This is expected since the dislocation mean spacing decreases with increasing the dislocation density, which is accumulated with increased plastic strain. This suggests that internal length scales decrease with the increase of the plastic strain level due to the additional amount of work hardening [24], while Eq. (19) suggests that the internal length l is proportional to the dislocation mean spacing.

3.2. Relating the internal length to dislocation spacing through discrete dislocation dynamics

Although it is difficult to capture the precise dislocation structure through experiments, discrete dislocation dynamics (DDD) simulations are a powerful method to investigate the plasticity and the underlying microstructure evolution at the submicron scale [32-36]. This method allows to tune the various dislocation characteristics, enabling the investigation of the macroscopic mechanical response dependence to dislocation parameters. In [37] aluminum crystals with two rigid (non-deforming) grain boundaries (tri-crystals), were simulated by DDD. The three cube shaped grains had the (100) direction as the loading direction and the grain boundary misorientation was 22.5°, the initial number of Frank-Read sources were constant, the dislocation source spacing was kept constant at 140 nm, and the dislocation source length was varied as (100 nm, 200 nm, and 300 nm), corresponding to initial dislocation densities (ρ) of $3.75\times10^{13}/m^2$, $7.5\times10^{13}/m^2$, and $10.25\times10^{13}/m^2$ [38, 39]. The initial dislocation mean spacing is given by $1/\sqrt{\rho}$, and was hence 163, 115, and 99 nm, respectively for the dislocation source lengths of 100 nm, 200 nm, and 300 nm. The dislocation density tensor profiles at a specific deformation state were also obtained [37-39]. According to the relationship between the dislocation density tensor and plastic strain gradient, the plastic strain distributions were derived from the DDD simulations for different values of the average strain [37-39]. Comparison between the plastic strain expressions predicted by strain gradient plasticity with the DDD simulation results provided values for the internal length scale, as deformation progressed and therefore gave an understanding of how the internal length depends on the strain [39]. For the cases where the dislocation source length was 200 nm and 300 nm, which were larger than the dislocation source spacing of 140 nm, it was shown that the plastic flow was controlled by the forest dislocation cutting mechanism. For this case the internal length decreased as the plastic strain increased (Fig. 1). Since as the strain increases the mean dislocation spacing decreases Fig. 1 suggests that the internal length is proportional to the dislocation spacing as was predicted by Eq. (19) [25].

3.3. Relating the internal length to the dislocation spacing through the Fleck-Hutchinson and Aifantis models

Recently, it was proposed [40] that a power law relationship is suitable to describe the evolution of the variable internal length with strain, which was documented by DDD [38]. Based on the Taylor hardening law the flow stress (σ_f) is related with the dislocation mean spacing L_S as

$$\sigma_f = Z\alpha Gb / L_S, \tag{22}$$

where b is the magnitude of the Burgers vector, α is a statistical coefficient (~ 0.3), G is the shear modulus and Z is the Taylor factor [24]. If a power-law relationship (same as Eq. (3)) is assumed for the stress-strain response then

$$\sigma_f = \kappa_0 \varepsilon^n. \tag{23}$$

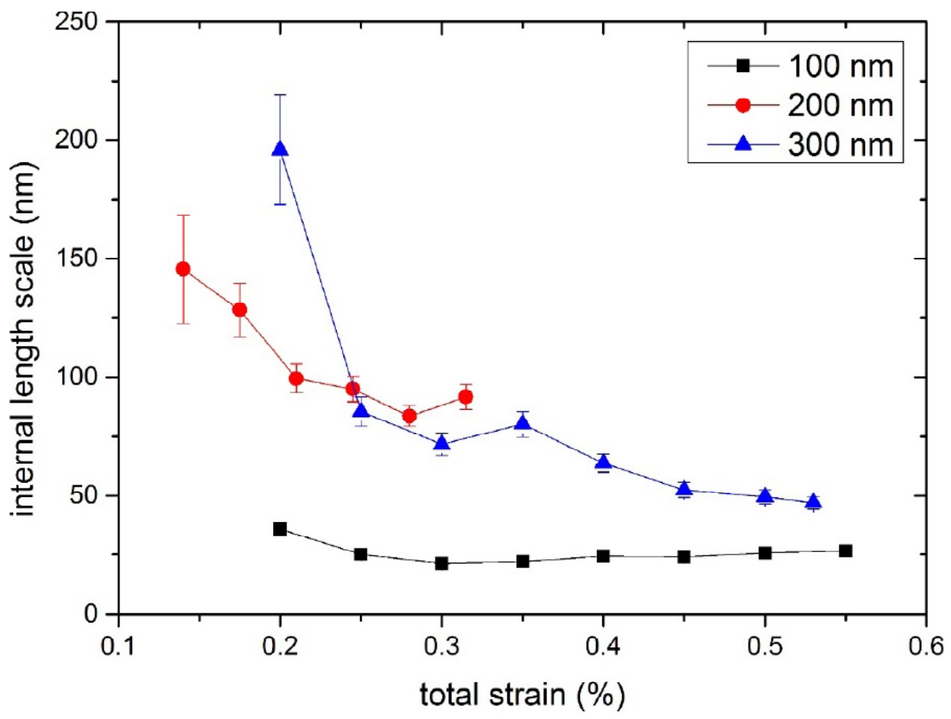

Fig. 1. Evolution of the internal length scale with increasing strain. Results obtained by comparing gradient plasticity with DDD simulations on tricrystals with different dislocation source lengths.

The physical description of the flow stress as expressed in Eq. (22) and the phenomenological description as expressed in Eq. (23) gave the connection between the dislocation mean spacing L_S and strain level as

$$L_S = \frac{Z\alpha Gb}{\kappa_0}\varepsilon^{-n}. \tag{24}$$

Motivated by the power law expression used in [31] Eq. (12) a strain dependent internal length scale was formulated as

$$l = l_0\varepsilon^{-n}. \tag{25}$$

l_0 is the internal length scale at shear strain equal to 1. Eq. (25) suggests that the internal length scale will decrease with increasing the strain level. Zhao et al. [40] further introduced the strain dependent internal length as expressed in Eq. (25) into Fleck et al.'s [18] strain gradient affected torsion solution and then successfully fit it to the torsion experiments. The obtained evolution of the internal length scale is shown in Figs. 2 and 3.

It should be noted here that if we use in Eq. (12) the relationship between the internal length and gradient coefficient $l(\bar{\varepsilon}) = \sqrt{c_2(\bar{\varepsilon})/\kappa_0}$ we can get

$$l(\bar{\varepsilon}) = l_0\bar{\varepsilon}^{\frac{n-1}{2}}. \tag{26}$$

It is interesting to note that although the Nix-Gao framework is formulated differently than the Aifantis and Fleck-Hutchinson models it can also yield an expression similar to Eqs. (25) and (26) as follows. They concluded [22] that the internal length is related to the flow stress σ_f as $l = b(G/\sigma_f)^2$ and since $\sigma_f = \kappa_0\varepsilon^n$ we can obtain

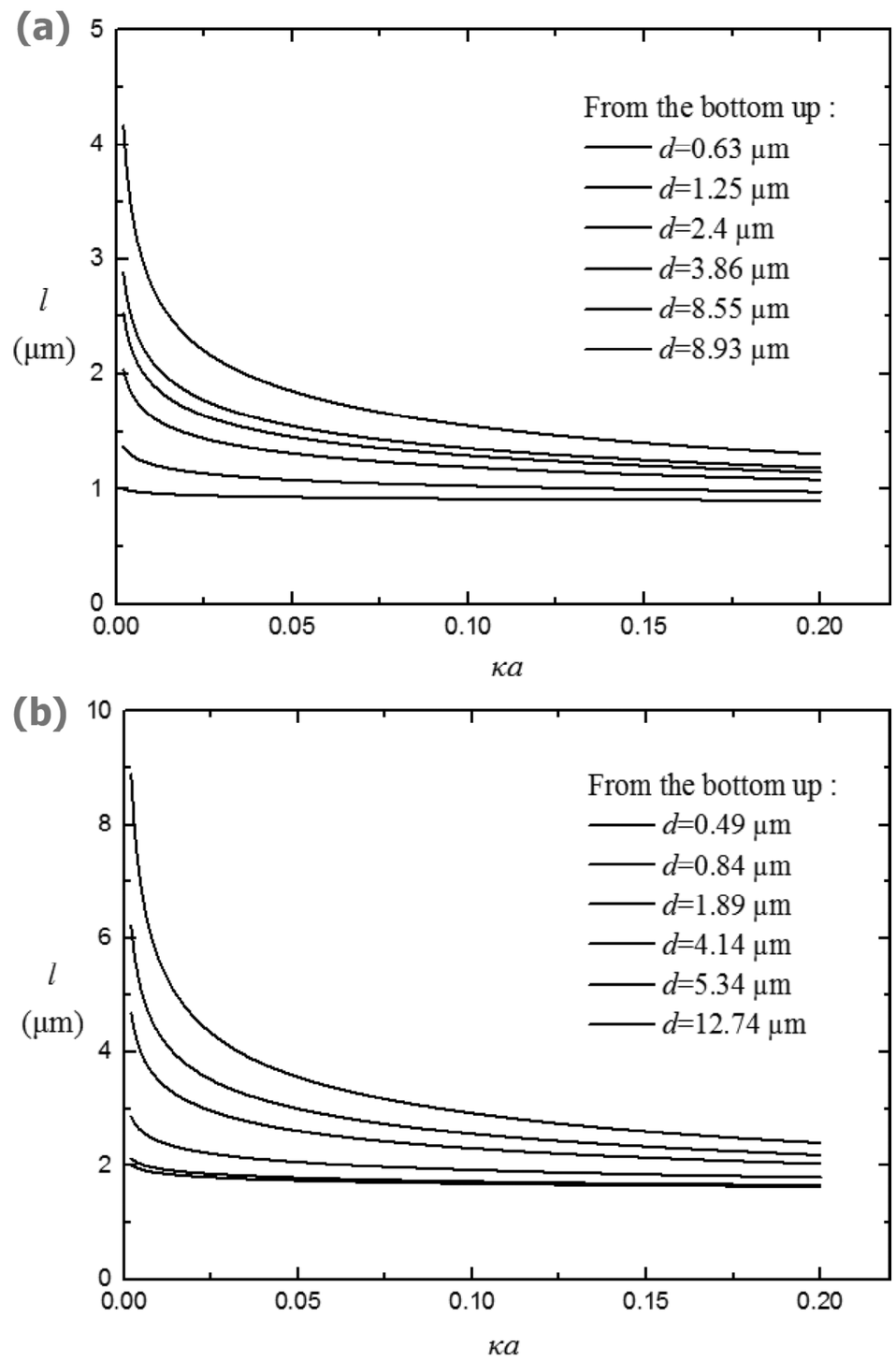

Fig. 2. The evolution of the internal length scale l with surface strain κa and its correlation with the grain size for torque-twist response of thin wires with the same diameter of (a) 20 μm (b) 50 μm but with different grain size d [40] (for the experiments of Gan *et al.* [53]).

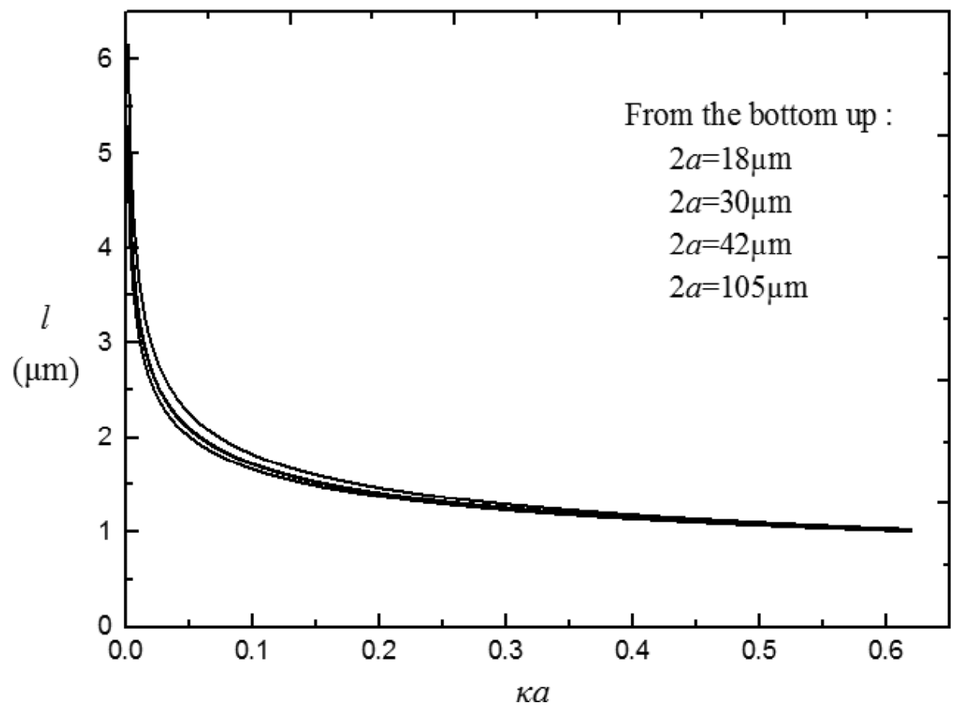

Fig. 3. The evolution of the internal length scale l with surface strain κa and its correlation with the sample size [40] (for the experiments of Liu *et al.* [54]).

$$l = b\left(G/\kappa_0\right)\varepsilon^{-2n} = l_0\varepsilon^{-2n}. \tag{27}$$

Eq. (27) is also similar as Zhao et al.'s expression in Eq. (25) and Aifantis's expression in Eq. (26).

Further studies, however, must be performed to clarify the difference of the value of the exponent in describing the strain dependent internal length scale in these three models (Eq. (25), (26), and (27)). Furthermore, it seems that there exists a strain independent internal length scale l_0 [22], however, this length scale in fact represents the internal length scale at strain level of 1.

It can therefore be concluded from this sub-section that the internal length scale decreases in a power-law [41] with strain, illustrating that the gradient influence on the size dependent mechanical response becomes weaker with increased plastic strain levels. This is consistent with the results summarized in Sections 3.1 and 3.2.

4. RELATING THE INTERNAL LENGTH WITH THE WITH THE DISLOCATION SOURCE LENGTH

From Fig. 1 it can be seen that if the source length was less than the initial dislocation spacing, then the plastic flow was controlled by the self-interaction of the source segments, and hence the plastic flow was nearly perfectly plastic. This was the case for the tri-crystals with a dislocation source length of 100 nm, which was smaller than the dislocation source spacing of 140 nm. For this case, as seen in Fig. 1, the internal length scale obtained by fitting the DDD data was constant at 25 nm throughout deformation and therefore was not dependent on the strain, as shown in Fig. 1. For the cases when dislocation source length of tri-crystals are of 200 nm and 300 nm, the underlying deformation mechanism was dislocation cutting mechanism, the internal length scales were related with dislocation mean spacing, rather than the dislocation source length (see Section 3.2).

5. RELATING THE INTERNAL LENGTH TO DISLOCATION PILE-UPS

Grain boundaries pose a resistance to dislocation movement and produce dislocation pileups, which in turn give rise to inhomogeneities in the plastic strain. Since the internal length scale represents the region over which the plastic strain gradient is significant, one can relate it with the pile-up length of dislocations in front of grain boundary. To do so gradient plasticity with an interface energy must be used.

In the one-dimensional case of the Aifantis-Willis model, by defining $\Phi = \gamma|\varepsilon^p|$ in Eq. (11) one can predict the stress at which grain boundaries will begin to deform plastically (grain boundary yield stress) [42,43] as

$$\sigma_c = \frac{\gamma}{2L}\coth\left(\frac{L}{l}\right), \tag{28}$$

where L is the grain size. The experimental value of the grain boundary yield stress Eq. (28) can be deduced from nanoindentation experiments [42-44], which exhibit a second strain burst in the load-displacement curve [42-44], indicating dislocation transmission/absorption across the grain boundary [42-44]. This second strain burst is dependent upon the indenter tip to grain boundary distance and therefore treating L in Eq. (28) as this distance allowed for fits to be obtained to experimental data. The fitted internal length scale was approximately 120 nm for Fe-2.2%Si [42].

In order to relate the internal length to the dislocation pileup length the following analysis was performed [42]. During nanoindentation dislocations initiate at the indenter tip and pileup at the grain boundary, and therefore the indenter tip to grain boundary distance can be viewed as the pile-up length ($L_{pile\text{-}up}$). At the onset of the second burst, indicating the yielding of grain boundary, the distance from the indenter to the grain boundary was estimated to be of the order of 200 nm (according to scanning electron microscopy images), and was related with the number of dislocation loops (n) in the pileup and the applied shear stress τ_a as

$$L_{pile-up} = \frac{nGb}{\pi\left(\tau_a - \tau_0\right)}, \tag{29}$$

where b was the magnitude of the Burgers vector (taken to be 0.25 nm), G was the shear modulus (taken to be 95 GPa), and τ_0 was the internal stress, which reflected the yielding of the grain interior and was calculated as one-sixth of the hardness at which the first strain burst occurred in the load - displacement curves. In Aifantis et al.'s work [42], by neglecting the internal stress τ_0 and estimating (from the experimental data) the applied shear stress as 1.5 GPa the number of dislocations in the pile-up was approximately calculated to be 40. The Distribution of 40 dislocations as shown in Fig. 4, suggested that the internal length scale of 120 nm covered 90% of the dislocation pile-up length.

Recently, Fe-3% Si alloy bicrystals with grain boundaries of different misorientation were investigated by Tsurekawa et al. [44], enabling the further investigation of the dependence of internal length scales on the grain boundary and dislocation struc-

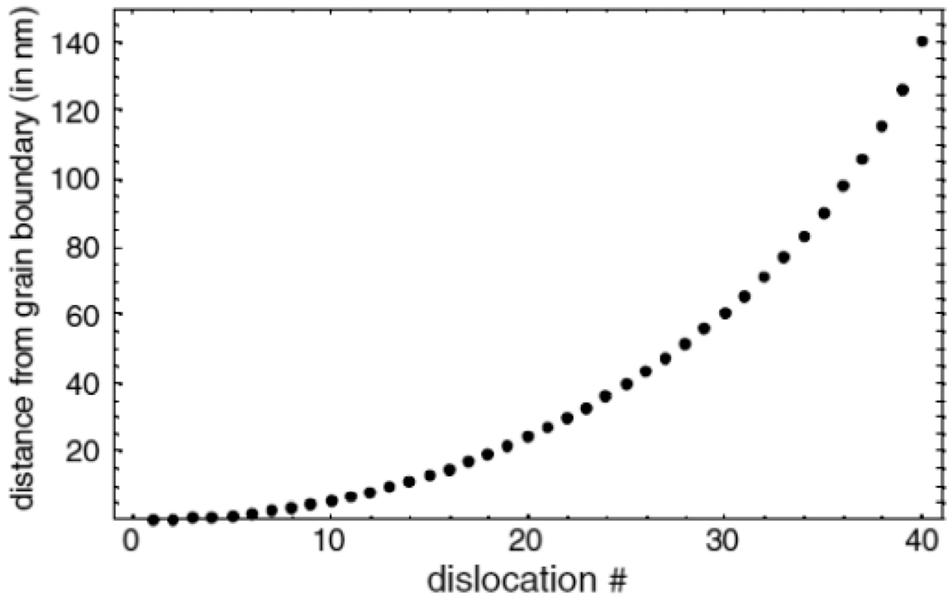

Fig. 4. Distribution of dislocation pile-ups in front of Fe-Si grain boundary during nanoindentation [42].

tures. Based on dislocation theory [45], the critical stress on the grain boundary during dislocation transference is the number of dislocations in the pileup (n) times the effective stress (τ_a- τ_0) due to the stress concentration

$$\tau_c = n\left(\tau_a - \tau_0\right). \tag{30}$$

Combination of Eq. (29) and (30) gives an alternative expression for the pile-up length as

$$L_{pile-up} = n^2 \frac{Gb}{\pi\tau_c}. \tag{31}$$

Tsurekawa et al. [44] calculated the critical stress τ_c and the number of pile-ups (n), and therefore Eq. (31) can be computed. Comparing the calculated pile-up length through dislocation theory Eq. (31) with the fitted internal length scales obtained from gradient plasticity Eq. (28), it was found that they are linearly proportional to each other and of the same order of magnitude. This is shown in Fig. 5 for Fe-3%Si with different grain boundaries [44].

6. RELATING THE INTERNAL LENGTH WITH THE DISTANCE BETWEEN DISLOCATION SOURCES

Interfacial yielding has also been observed during nanoindentation near grain boundaries of Nb polycrystals. Performing a fit of Eq. (28) as was described for the Fe-Si data yielded an internal length of 1.4 μm for Nb [43]. This value is (a) close to the distance between dislocation sources in pure crystals, (b) significantly larger than the internal length for the Fe-Si alloys. This led to the suggestion that the internal length is related to the distance between dislocation sources [43]. Particularly, for pure metals, the distance between dislocation sources is ~1 μm, while due to the existence of impurities in

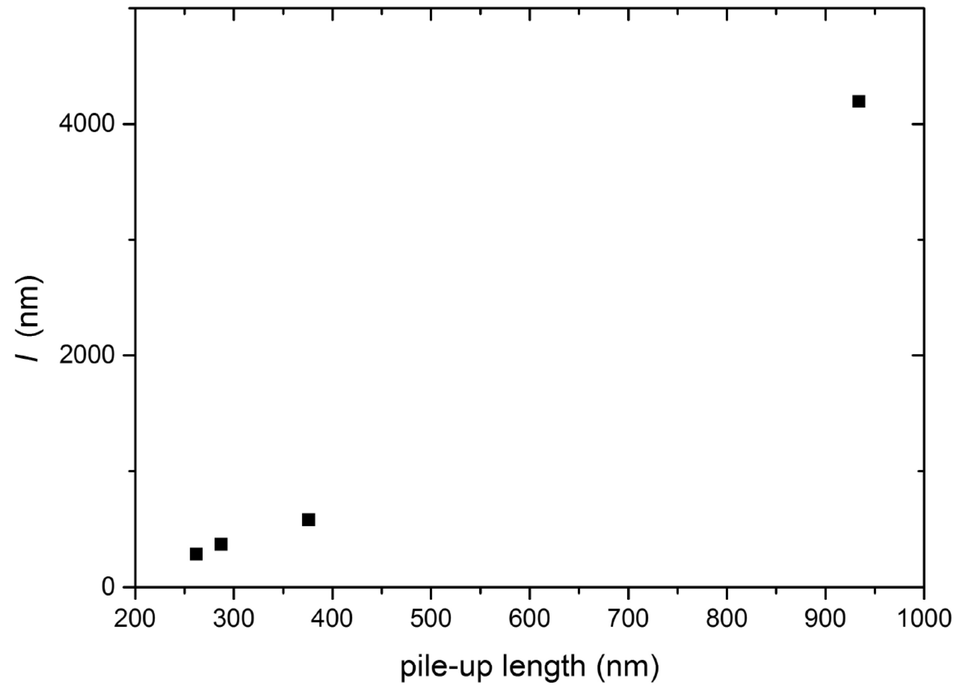

Fig. 5. Relationship between internal length l with pile-up length $L_{pile-up}$ in front of GB during nanoindentation in Fe-Si [46].

Fe-Si alloy, the distance between dislocation sources is expected to be one order smaller than that of pure metals. Furthermore, the greater the Si content the smaller the distance between dislocation sources and hence the internal length should decrease with increasing the wt.%Si if indeed it is related to the distance between dislocation sources. This is consistent with the observation that if the initial distance between the indenter tip to grain boundary is used in Eq. (28) as L, then the internal length for the Fe-2.2wt.% Si was found to be 422 nm [46] while for the Fe-3wt.%Si it was significantly smaller (between 101 nm and 223 nm depending on the grain boundary misorientation [46]). It should be noted here that a smaller distance between dislocation sources corresponds to a smaller distance between the dislocation spacing, only if the initial dislocation source length is also the same.

7. RELATING THE INTERNAL LENGTH TO THE SAMPLE MICROSTRUCTURE

In addition to a dependence of the internal length on dislocation characteristics it can also be related to the microstructure and specimen size. Some results in this directions are summarized below.

7.1. Relationship between the internal Length and slip zone thickness

In addition to the effects that the underlying microstructure, specimen size and dislocation dynamics can have on the internal length, it is possible that the theoretical modeling employed can affect its value. Such an example is summarized here. The unique serrated stress-strain response, observed in micropillar compression experiments [47-49], re-

mained an unresolved issue from a modeling point of view until strain gradient plasticity was employed [8]. Scanning electron microscopy imaging illustrated that the micropillar deformation was heterogeneous, and slip zones formed during deformation. This motivated Zhang and Aifantis [8] to model the stress-strain response of micropillars by allowing the pillar to yield in sequential layers, i.e. the yield stress was taken to vary along the pillar axis. A multilayer strain gradient model was proposed and a strain burst occurred when two neighboring layers yielded consecutively. Hence, the number of the strain bursts observed in the stress-strain curve was determined by the number of the layers into which the pillar was divided into. The model was in perfect agreement with the experimental data and it was found that the fitted internal length scale values were similar to the thickness of the layers. Increasing the layer thickness resulted in larger values for the fitted internal length. The layer thickness was dependent on the number of the observed strain bursts that was necessary to model. Hence, the more strain busts the more layers the pillar had to be divided into, and the smaller their thickness.

Another characteristic deformation of micropillar compression is that the stress-strain response of same diameter pillars are scattered due to the stochasticity of the microstructure [47-49]. The proposed multilayer strain gradient plasticity model was used to capture the upper and lower bounds of the dispersed experimentally measured stress–strain curves [7]. The fitted internal length scales were again found to be of the same order of layer thickness, and particularly the internal length scales were proportional to it.

These aforementioned observations are expected since the internal length scale in strain gradient plasticity theory is a parameter accounting for the characteristic region over which heterogeneous deformation is pronounced, i.e. the strain gradient effect is significant. In the multilayer strain gradient model, the strain gradient effect is constrained within the separate layers, which are the main microstructure indicative of the heterogeneous deformation.

The stochastic occurrence of strain bursts, was further captured introducing a randomly distributed yield-stress following a Weibull distribution into the multilayer strain gradient plasticity model [9]. The stochasticity enriched multilayer strain gradient plasticity model was implemented with the aid of cellular automaton simulations [10,50,51]. The cellular automaton allowed more layers to be modeled and hence more strain bursts to be captured. However, in this case the number of layers that the simulation can handle can affect the internal length, and therefore computational power can come into play. The internal length scales, which were obtained from the comparison of strain gradient plasticity with the experimentally measured serrated stress-strain response of micropillar compression is plotted in Fig. 6. It should be noted that a 2 μm tall pillar could be modeled with five layers of ~0.52 μm, while a 15 μm tall pillar could also be modeled with such a layer thickness. In both cases as seen in Fig. 6 the internal length was predicted to be the same regardless of the length, hence size did not affect it. Furthermore, in Fig. 6 it is seen that the internal length scale is proportional to the layer thickness.

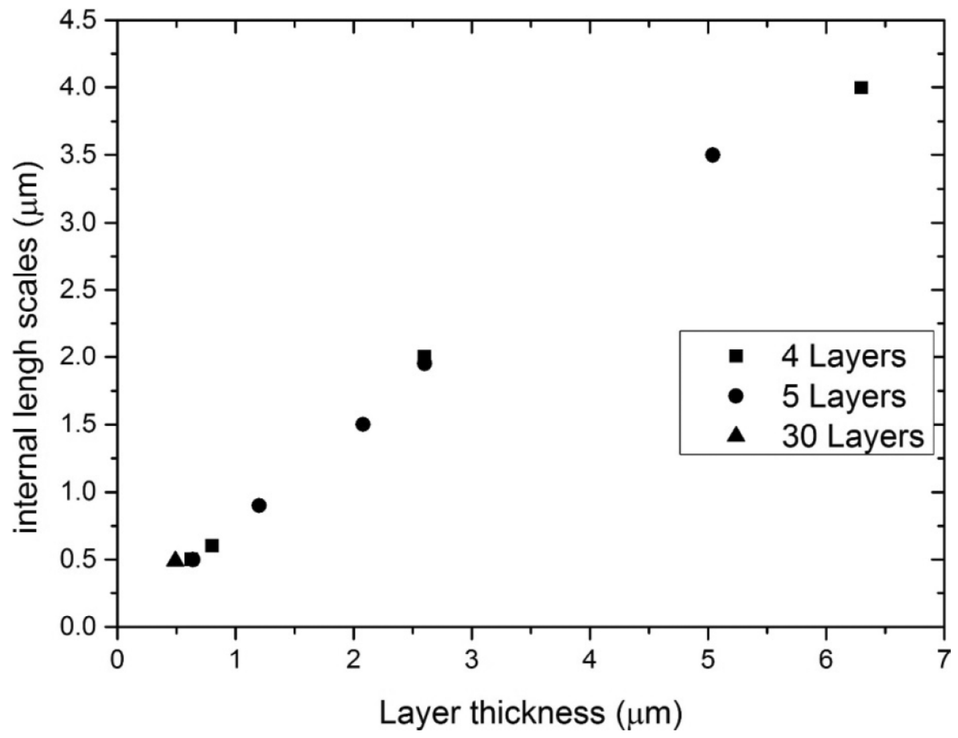

Fig. 6. Relationship between internal length scale and the layer thickness of single crystal micropillar. (Data plotted from [7-9]).

7.2. Relating the internal length with the grain size

If there is a grain boundary parallel to the pillar axis of the compressed micropillar, then instead of the serrated strain bursts or stress drops there are two “knees” in the smooth stress-strain curves, which are hence tri-linear [7,52]. The first knee denotes grain yielding, while the second knee indicates grain boundary yielding, as was predicted by gradient plasticity with interface effects [28-29]. Therefore, the previously derived stress-strain solutions [28-29] were successfully fit to these experimental data [7]. The internal length scale values ranged between (2.8-5.1 μm) which was comparable to the pillar radius (3 μm) [7]. It’s reasonable that the heterogeneous deformation developed across the whole section of the micropillar due to the grain boundary’s opposition to the movement of dislocations. Thus the pile-up length was almost half of the sample diameter (and equal to the grain size).

Zhao et al. [40] further investigated the correlation between the internal length scales and the grain size for polycrystalline samples. Based on the power law relationship for the internal length Eq. (25), the classical Fleck-Hutchinson strain gradient theory was generalized to consider a variable internal length scale. This model was able to capture tension and torsion experiments of annealed gold wires with diameters of 20 μm and 50 μm containing different grain sizes [53]. Such a comparison suggested that the internal length at the onset of deformation was a configuration-dependent parameter, and was closely related to the grain size as shown in Fig. 2. Such a correlations can be attributed to the material's ductility since the strain hardening exponents as defined in Eq. (23) accounts for it. Particularly, for polycrystalline materials, it was found that decreasing the grain size usually improves the material's strength according to the Hall-Petch relation, while causing the ductility to decrease due to the limited capacity of grains to store dislocations [3], hence increasing the ductility (larger grain size) gives a larger internal length. (It should be mentioned that the inverse Hall-Petch [3,5] will occur at grain sizes less than about ~15 nm (depending on the material), but such small sizes were not considered in the torsion experiment documented above [53].)

The observation that the initial internal length is larger for polycrystalline materials with larger grain size is consistent with the suggestion of Gracio [55] and Voyiadjis&Abu Al-Rub [56]. They speculated that the mean free path of dislocations at the initial deformation stage is of the order of the grain size and then decreased to a constant value on the order of micrometers after a strain of about only 0.1 [55]. Thus the larger the grain size, the larger the dislocation mean free path and the corresponding initial internal length.

7.3. Connection with specimen-size

More recently, the generalized Fleck-Hutchinson strain gradient theory was successfully used [40] to capture tension and torsion experiments performed on annealed polycrystalline copper wires (99.999% purity) with diameters ranging from 18 μm to 105 μm, while the grain size was almost the same in all samples [54]. In this work the internal length scale was allowed to vary with increasing strain and it was found that the sample size affects the initial value of the internal length scale; the larger the pillar diameter, the larger the initial internal length scale, as shown in Fig. 3 [40]. The strain-hardening exponent, which is a reflection of material ductility, is the bridge between such a dependence since it is related to both the internal length scale and the sample size. It has been experimentally observed that larger samples are more ductile than smaller ones, since smaller material volumes are sensitive to the development of defects which results in material failure [40]. It's also found that the internal length scale is almost the same for all deformed samples at a high strain level, since the dislocation mean spacing is almost constant once the saturated dislocation density limit was reached. This again indicates the relationship of the internal length to the dislocation spacing, as described in Section 3.

8. CONCLUSIONS

Internal length scales are an important parameter in strain gradient plasticity framework. They enter into strain gradient plasticity framework through either the modified flow stress or modified effective strain or energy. Their introduction enabled the interpretation of the mechanical behavior of numerous micron and nanostructures. However, the physical meaning of the internal length and its connection to the underlying microstructure is at best tenuous. Comparison between strain gradient plasticity models with simulation and experimental results has shown that the internal length scale vary throughout deformation and are proportional to the dislocation mean spacing, dislocation pile-up length, distance between dislocation sources, thickness of slip bands, grain size and even sample size. However, a comprehensive examination on how the internal length is related to all the aforementioned parameters has not been performed. Therefore, further simulations and experiments should be performed. Furthermore, the overviewed studies are limited to static loading at room temperature. However, in addition to the strain dependence of the internal length scale, its dependence on the strain rate and temperature which are particularly important in problems of creep, recrystallization, and dynamic shear banding [1] but also be examined through new systematic experiments and simulation efforts.

ACKNOWLEDGEMENT

XZ is grateful for the support of NSFC (11202172), CPSF (2013M530405), the Basic Application Research Plan of Sichuan Province (2015JY0239) and the Sichuan Provincial Youth Science and Technology Innovation Team (2013TD0004).

REFERENCES

[1] E.C. Aifantis // *Mech. Mater.* **35** (2003) 259.
[2] N.A. Fleck and J.W. Hutchinson // *J. Mech. Phys. Solids* **49** (2001) 2245.
[3] M.A. Meyers, A. Mishra and D.J. Benson // *Prog. Mater Sci.* **51** (2006) 427.
[4] K.E. Aifantis and A.A. Konstantinidis // *Mater. Sci. Eng. A* **503** (2009) 198.
[5] X. Zhang and K.E. Aifantis // *J. Mater. Res.* **26** (2011) 1399.
[6] X. Zhang and K.E. Aifantis // *Reviews on Advanced Materials Science* **26** (2010) 74.
[7] X. Zhang, K.E. Aifantis and A.H.W. Ngan // *Materials Science and Engineering: A* **591** (2014) 38.
[8] X. Zhang and K.E. Aifantis // *Materials Science and Engineering: A* **528** (2011) 5036.
[9] A.A. Konstantinidis, K.E. Aifantis and J.T.M. De Hosson // *Materials Science and Engineering: A* **597** (2014) 89.
[10] A.A. Konstantinidis, X. Zhang and E.C. Aifantis // *AIP Conf. Proc*. **1646** (2015) 3.
[11] E.C. Aifantis // *Journal of Engineering Materials and Technology-Transactions of the ASME* **106** (1984) 326.
[12] E.C. Aifantis // *Int. J. Plast.* **3** (1987) 211.
[13] H.M. Zbib and E.C. Aifantis // *Scr. Metall.* **22** (1988) 703.
[14] H.M. Zbib and E.C. Aifantis // *Res Mechanica* **23** (1988) 293.
[15] H.M. Zbib and E.C. Aifantis // *Res Mechanica* **23** (1988) 261.
[16] H.M. Zbib and E.C. Aifantis // *Res Mechanica* **23** (1988) 279.
[17] LJ. Sluys and R. de Borst // *Mech. Mater.* **18** (1994) 131.
[18] N.A. Fleck, G.M. Muller, M.F. Ashby and J.W. Hutchinson // *Acta Metall. Mater.* **42** (1994) 475.
[19] N. Taheri-Nassaj and H.M. Zbib // *Int. J. Plast.* (2015), to be published.
[20] J.W. Hutchinson // *Int. J. Solids Struct.* **37** (2000) 225.
[21] E. Kröner // *Int. J. Eng Sci* **1**(1963) 261.
[22] W.D. Nix and H. Gao // *J. Mech. Phys. Solids* **46** (1998) 411.
[23] H. Gao, Y. Huang, W.D. Nix and J.W. Hutchinson// *J. Mech. Phys. Solids* **47** (1999) 1239.
[24] R.K. Abu Al-Rub and G.Z. Voyiadjis // *Int. J. Plast.* **20** (2004) 1139.
[25] P. Gudmundson // *J. Mech. Phys. Solids* **52** (2004) 1379.
[26] M.E. Gurtin and L. Anand // *J. Mech. Phys. Solids* **53** (2005) 1624.
[27] M.E. Gurtin and L. Anand // *J. Mech. Phys. Solids* **57** (2009) 405.
[28] K. Aifantis and J.R. Willis, In: *Proc. 7th Nat. Congr. Mech.* (2004), p. 372.
[29] K.E. Aifantis and J.R. Willis // *J. Mech. Phys. Solids* **53** (2005) 1047.
[30] M.R. Begley and J.W. Hutchinson // *J. Mech. Phys. Solids* **46** (1998) 2049.
[31] L. Tsagrakis and E.C. Aifantis // *Journal of Engineering Materials and Technology, Transactions of the ASME* **124** (2002) 352.
[32] H. Fan, Z. Li, M. Huang and X. Zhang // *Int. J. Solids Struct.* **48** (2011) 1754.
[33] M. Huang and Z. Li // *J. Mech. Phys. Solids* **61** (2013) 2454.
[34] M. Huang, Z. Li and J. Tong // *Int. J. Plast.* **61** (2014) 112.
[35] H.M. Zbib and T. Diaz de la Rubia // *Int. J. Plast.* **18** (2002) 1133.
[36] V.V. Bulatov and W. Cai, *Computer Simulations of Dislocations* (Oxford University Press, 2006).
[37] K.E. Aifantis, J. Senger, D. Weygand and M. Zaiser // *IOP Conference Series: Materials Science and Engineering* **3** (2009) 012025.
[38] X. Zhang, K.E. Aifantis, J. Senger, D. Weygand and M. Zaiser // *J. Mater. Res.* **29** (2014) 2116.
[39] X. Zhang and K.E. Aifantis // *Materials Science and Engineering: A* **631** (2015) 27.
[40] J. Zhao, X. Zhang, A.A. Konstantinidis and G. Kang // *Philos. Mag. Lett.* **95** (2015) 340.
[41] X. Zhang, J. Zhao, A.A. Konstantinidis and E. Aifantis // Submitted to *Philos. Mag*.
[42] K.E. Aifantis, W.A. Soer, J.T.M. De Hosson and J.R. Willis // *Acta Mater.* **54** (2006) 5077.
[43] K.E. Aifantis and A.H.W. Ngan // *Mater. Sci. Eng. A* **459** (2007) 251.
[44] S. Tsurekawa, Y. Chihara, K. Tashima, S. Ii and P. Lejcek// *Journal of Materials Science* **49** (2014) 4698.
[45] J.P. Hirth and J. Lothe, *Theory of Dislocations*, second ed. (Wiley, New York, 1982).
[46] X. Zhang, K.E. Aifantis and S. Tsurekawa // submitted to *Materials Science and Engineering: A*.
[47] M.D. Uchic, D.M. Dimiduk, J.N. Florando and W.D. Nix // *Science* **305** (2004) 986.

[48] J.R. Greer // *Reviews on Advanced Materials Science* **13** (2006) 59.
[49] J.R. Greer and J.T.M. De Hosson // *Prog. Mater Sci.* **56** (2011) 654.
[50] K.E. Aifantis, A. Konstantinidis and S. Forest // *Journal of Computational and Theoretical Nanoscience* **7** (2010) 360.
[51] X. Zhang, K.E. Aifantis and M. Zaiser // *Reviews on Advanced Materials Science* **35** (2013) 39.
[52] K.S. Ng and A.H.W. Ngan // *Philos. Mag.* **89** (2009) 3013.
[53] Z. Gan, Y. He, D. Liu, B. Zhang and L. Shen // Scripta Mater. **87** (2014) 41.
[54] D. Liu, Y. He, X. Tang, H. Ding, P. Hu, P. Cao // *Scripta Mater.*, **66** (2012)406-409.
[55] J.J. Gracio // *Scripta Metallurgica Et Materialia* **31** (1994) 487.
[56] G.Z. Voyiadjis and R.K. Abu Al-Rub // *Int. J. Solids Struct.* **42** (2005) 3998.
[57] J.G. Swadener, E.P. George and G.M. Pharr // *J. Mech. Phys. Solids* **50** (2002) 681.
[58] J.G. Swadener, A. Misra, R.G. Hoagland and M. Nastasi // *Scripta Mater.* **47** (2002) 343.
[59] Y.L. Lim, A.J. Bushby and M. Chaudhri // *Fundamentals of Nanoindentation and Nanotribology* (1998)145.
[60] Y.Y. Lim and M.M. Chaudhri // *Philosophical Magazine A-Physics of Condensed Matter Structure Defects and Mechanical Properties* **79** (1999) 297.